

# Search for Cosmic-Ray Produced Dark Meson via the $U(1)_D$ Portal at JUNO

---

**Zirong Chen,<sup>a</sup> Dan Chi,<sup>b</sup> Jinmian Li,<sup>a</sup> Junle Pei<sup>c</sup>**

<sup>a</sup>*College of Physics, Sichuan University, Chengdu 610065, China*

<sup>b</sup>*Provincial Key Laboratory of Solid-State Optoelectronic Devices, Zhejiang Normal University, Jinhua, 321004, China*

<sup>c</sup>*Institute of Physics, Henan Academy of Sciences, Zhengzhou 450046, China*

*E-mail:* [chenzirong@stu.scu.edu.cn](mailto:chenzirong@stu.scu.edu.cn), [chidan@zjnu.edu.cn](mailto:chidan@zjnu.edu.cn),  
[jmli@scu.edu.cn](mailto:jmli@scu.edu.cn), [peijunle@hinas.ac.cn](mailto:peijunle@hinas.ac.cn)

**ABSTRACT:** We investigate the atmospheric production and subsequent detection of sub-GeV dark mesons within the framework of a confining dark sector coupled to the Standard Model (SM) via a  $U(1)_D$  vector portal. High-energy cosmic ray interactions in the atmosphere produce dark quarks through proton bremsstrahlung, rare decay of Standard Model mesons, and Drell-Yan processes, which subsequently hadronize into dark mesons. We adopt a modified Quark Combination Model to describe the non-perturbative dark hadronization process, allowing for a detailed event-level characterization of the dark meson flux. We simulate the flux and the interaction of these relativistic dark mesons in the Jiangmen Underground Neutrino Observatory (JUNO) using the GENIE generator, considering both elastic scattering off nuclei and deep inelastic scattering channels. Based on the projected 20 kton·year exposure, we derive sensitivity limits on the coupling strength between the dark gauge boson and the SM sector. Our results demonstrate that JUNO can probe substantial unexplored parameter space, particularly for light mediators ( $m_{Z'} \lesssim 10$  MeV), where it achieves sensitivities to the portal interaction as low as  $2.4 \times 10^{-4}$ .

---

## Contents

<b>1</b>	<b>Introduction</b>	<b>1</b>
<b>2</b>	<b>The Dark Matter Model</b>	<b>3</b>
2.1	The $U(1)_D$ Portal Interaction	3
2.2	Dark Mesons and Chiral Symmetry Breaking	3
<b>3</b>	<b>From Quark to Meson: modified Quark Combination Model</b>	<b>7</b>
<b>4</b>	<b>Productions of Dark Gauge Boson and Dark Meson</b>	<b>10</b>
4.1	Proton Bremsstrahlung Production	10
4.2	SM Meson Decay	12
4.3	Drell-Yan Production of Dark Quark	13
4.4	Overall Flux of Dark Meson	15
<b>5</b>	<b>DM-Nucleus Scattering at The JUNO Detector</b>	<b>16</b>
5.1	Simulation Framework with GENIE	16
5.2	Cross-Section Calculation and Event Generation	17
5.3	Signal Selection and Sensitivity at JUNO	18
<b>6</b>	<b>Conclusions</b>	<b>20</b>

---

## 1 Introduction

The Standard Model (SM) of particle physics has achieved remarkable success in describing fundamental interactions. However, it fails to explain the existence of Dark Matter (DM). While Weakly Interacting Massive Particles (WIMPs) have long been the leading candidates, the null results from direct detection experiments and the Large Hadron Collider (LHC) have motivated the exploration of alternative paradigms, particularly those involving light dark sectors in the sub-GeV mass range [1]. A theoretically well-motivated class of such models involves a “Hidden Valley” or a strongly interacting dark sector, characterized by a new non-Abelian gauge group  $SU_D(N)$  [2–5]. Analogous to Quantum Chromodynamics (QCD), this dark sector confines at low energies, giving rise to a rich spectrum of dark hadrons. Among those bound states, the lightest dark hadrons, which are often identified as pseudo-Nambu-Goldstone bosons or “dark pions” ( $\pi_D$ ) [6–11], can be stable and serve as viable dark matter candidates. This scenario naturally realizes the Strongly Interacting Massive Particle (SIMP) mechanism [12–15], which not only provides the correct relic abundance but also offers a potential solution to the small-scale structure problem [16, 17].

The phenomenology of these strongly interacting dark sectors heavily depends on the portal connecting them to the visible sector. A minimal and predictive scenario is established via the kinetic mixing between a new  $U(1)_D$  gauge boson and the SM photon [18, 19]. Through this vector portal, dark quarks can be produced in high-energy collisions, subsequently hadronizing into dark mesons. Extensive constraints on such scenarios have been placed by accelerator-based beam dump experiments and collider searches, which target signatures such as displaced vertices induced by the long-lived dark meson [20–27], semi-visible jets [28–33], emerging jets [34–38] and so on. Complementary to terrestrial accelerators, high energy cosmic rays colliding with the Earth’s atmosphere (also dubbed as cosmic-ray air shower) provide a complementary and permanent source of sub-GeV dark sector particles [39–45]. This atmospheric production mechanism has been extensively studied for Millicharged Particles (MCPs) [46–51], but its application to composite dark sectors remains less explored due to the complexities arising from the non-perturbative dark hadronization process.

In this work, we investigate the atmospheric production and subsequent detection of sub-GeV scale dark mesons within the framework of a dark  $SU(N)$  gauge theory coupled to the SM via a  $U(1)_D$  portal. We will focus on the coupling between the new gauge boson and the SM quark [52–56]. The leptonic couplings can be assumed to be suppressed to evade the stringent bounds from electron beam dump and lepton collider experiments. We construct the low-energy effective Lagrangian based on Chiral Perturbation Theory (ChPT) to describe the dynamics of the dark pions. The flux of dark mesons originating from cosmic-ray proton interactions is calculated by considering three distinct production channels: proton bremsstrahlung, the decay of SM mesons (specifically  $\pi^0$ ,  $\eta$ ) into dark gauge boson, and the Drell-Yan production of dark quarks.

A critical challenge in modeling the flux of composite dark matter is the description of the hadronization process from dark quarks to dark mesons. Unlike previous studies that often rely on phenomenological hadronization model or generic scaling of PYTHIA parameters [57, 58] to approximate a confining  $SU(N)$  gauge interaction, we employ a Modified Quark Combination Model (MQCM) [3, 59–63] to describe the hadronization process. Under the assumption of an approximate flavor symmetry within the dark sector, this framework enables a detailed, event-by-event characterization of the multiplicity and kinematics of dark mesons generated in atmospheric dark showers.

Once produced, these relativistic dark mesons travel through the Earth and can scatter off electrons or nuclei in deep underground detectors. The Jiangmen Underground Neutrino Observatory (JUNO) [64–66], with its large fiducial mass (20 kton) and excellent energy resolution, offers an ideal environment for probing such light, weakly interacting particles. We calculate the scattering rates of the atmospheric dark mesons flux within the JUNO detector utilizing the boosted dark matter module [67, 68] implemented in the GENIE framework [69, 70], thereby deriving projected sensitivity limits on the model parameter space.

The remainder of this paper is organized as follows. In Section 2, we outline the theoretical framework of the dark  $SU(N)$  model and construct the effective Lagrangian for dark pions. Section 3 elaborates on the implementation of the MQCM. Section 4 details the

calculation of the atmospheric dark meson flux, incorporating contributions from proton bremsstrahlung, SM meson decay, and Drell-Yan production. In Section 5, we describe the evaluation of signal event rate at JUNO and present the projected sensitivities. Finally, we summarize our findings and discuss their implications in Section 6.

## 2 The Dark Matter Model

Analogous to the QCD in the SM, we postulate a dark sector governed by a non-Abelian  $SU(N)_D$  gauge interaction, which exhibits both asymptotic freedom and dark quark confinement. The Lagrangian density for dark quarks and dark gluons is given by:

$$\mathcal{L}_{\text{dQCD}} = -\frac{1}{4}G_{\mu\nu}^a G_a^{\mu\nu} + \sum_{k,j=1}^{N_f} \bar{q}_k (i\cancel{D} \delta_{k,j} - m_{k,j}) q_j , \quad (2.1)$$

where  $G_{\mu\nu}^a$  ( $a = 1, 2, \dots, N^2 - 1$ ) denotes the field strength tensor of the dark gluons, and  $M_q = (m_{k,j})$  is the mass matrix for the  $N_f$  dark quark flavors. For simplicity, we assume a diagonal mass matrix:

$$M_q = \text{diag}(m_1, m_2, \dots, m_{N_f}) . \quad (2.2)$$

### 2.1 The $U(1)_D$ Portal Interaction

We introduce a dark  $U(1)_D$  gauge symmetry that mediates interactions between the dark quarks and the SM quark. The interaction Lagrangian for the dark quarks is:

$$\mathcal{L}_{\text{int}} \supset -g' Z'_\mu \sum_{k=1}^{N_f} \bar{q}_k \gamma^\mu (Q'_{k,L} P_L + Q'_{k,R} P_R) q_k , \quad (2.3)$$

where  $Z'_\mu$  and  $g'$  represent the dark gauge field and its associated gauge coupling, respectively. The parameters  $Q'_{k,L/R}$  denote the  $U(1)_D$  charges of the left- and right-handed dark quarks  $q_{k,L/R}$ .

To establish a portal to the SM, the  $Z'$  boson couples to the SM quarks as follows:

$$\mathcal{L}_{\text{int}} \supset -g_{\text{SM}} Z'_\mu \bar{\psi}_f \gamma^\mu \psi_f , \quad (2.4)$$

where  $f = \{u, d, s, c\}$  denotes the light SM quark flavors relevant to our analysis. For simplicity, the  $U(1)_D$  charges of SM fermions are absorbed into the effective coupling  $g_{\text{SM}}$ . We assume purely vector-like couplings to the SM and require the  $Z'$  to be lepton-phobic to evade stringent constraints from lepton beam dump and collider experiments.

### 2.2 Dark Mesons and Chiral Symmetry Breaking

In the case where dark quark masses are zero, the Lagrangian density in Eq. (2.1) exhibits independent chiral symmetry between the left-handed and right-handed quark fields, enabling independent  $SU(N_f)_L$  and  $SU(N_f)_R$  transformations. It also possesses  $U(1)_V$  symmetry for global phase transformations and  $U(1)_A$  symmetry for axial transformations, the latter at a classical level. The global symmetry is described by

$$U(N_f)_L \times U(N_f)_R = SU(N_f)_L \times SU(N_f)_R \times U(1)_V \times U(1)_A . \quad (2.5)$$

When a non-zero dark-quark condensate  $\langle \bar{q}q \rangle$  forms at an energy scale below the confinement scale  $\Lambda_{\text{dQCD}}$ , the chiral symmetry  $SU(N_f)_L \times SU(N_f)_R$  undergoes spontaneous symmetry breaking to a vector symmetry  $SU(N_f)_V$ ,

$$SU(N_f)_L \times SU(N_f)_R \rightarrow SU(N_f)_V . \quad (2.6)$$

According to the pattern of spontaneous symmetry breaking in Eq. (2.6), Goldstone bosons, identified as dark mesons  $\pi_a$  ( $a = 1, 2, \dots, N_f^2 - 1$ ), are generated. These dark mesons remain massless in the limit where dark quark masses are absent. However, due to the explicit breaking of chiral symmetry by the dark quark masses in Eq. (2.2), the dark mesons acquire small masses.

At the lowest order, these dark mesons can be effectively described by the  $\sigma$  model, with the Lagrangian density given by

$$\mathcal{L}_{\text{eff}} = \frac{F_0^2}{4} \text{Tr}[(D_\mu U)(D^\mu U)^\dagger] + \frac{F_0^2 B_0}{2} \text{Tr}[M_q U^\dagger + U M_q^\dagger] , \quad (2.7)$$

where

$$U = e^{\frac{2i}{F_0} \pi_a T^a} . \quad (2.8)$$

In this expression,  $F_0$  represents the decay constant of the dark mesons, and  $T^a$  ( $a = 1, 2, \dots, N_f^2 - 1$ ) are the generators of the  $SU(N_f)$  group.

Based on the chirality of the fermions, we represent the dark quark fields as

$$q_k = \begin{pmatrix} q_{k,L} \\ q_{k,R} \end{pmatrix} . \quad (2.9)$$

We define

$$2\pi_a T^a + \sqrt{\frac{2}{N_f}} \eta_1 I_{N_f \times N_f} = \sqrt{2}\pi' , \quad (2.10)$$

where  $I_{N_f \times N_f}$  is the  $N_f \times N_f$  identity matrix. The correspondence between the matrix elements of  $\pi'$  and the dark quark fields is given by

$$\pi'_{k,j} \longleftrightarrow i\bar{q}_k \gamma^5 q_j = i \left( q_{k,L}^\dagger q_{j,R} - q_{k,R}^\dagger q_{j,L} \right) . \quad (2.11)$$

Under the transformations of parity ( $\hat{P}$ ) and charge conjugation ( $\hat{C}$ ), these fields satisfy

$$\hat{P}\pi'_{k,j}\hat{P} = -\pi'_{k,j} , \quad (2.12)$$

$$\hat{C}\pi'_{k,j}\hat{C} = \pi'_{j,k} . \quad (2.13)$$

In conclusion, these dark mesons exhibit pseudoscalar characteristics, as evidenced by their transformations under parity and charge conjugation.

The matrix elements of  $\pi'$  or the combinations of these elements lead to  $N_f^2 - 1$  dark mesons  $\pi_a$  and a singlet meson  $\eta_1$ . When  $k \neq j$ ,  $\pi'_{k,j}$  corresponds to complex neutral

and charged dark mesons, totaling  $N_f^2 - N_f$ . For instance, in QCD with  $N_f = 3$ , we find  $\pi'_{1,2/2,1} = \pi^\pm$ ,  $\pi'_{1,3/3,1} = K^\pm$ , and  $\pi'_{2,3/3,2} = K^0/\bar{K}^0$ . According to Eq. (2.7), we have the squared masses of  $\pi'_{k,j}$  as

$$M_{\pi'_{k,j}}^2 = B_0(m_k + m_j) , \quad k \neq j . \quad (2.14)$$

Among  $\pi_a$  ( $a = 1, 2, \dots, N_f^2 - 1$ ), we denote the real neutral dark mesons as  $\pi_A$  ( $A = 1, 2, \dots, N_f - 1$ ), which are related to  $\pi'_{k,k}$  ( $k = 1, 2, \dots, N_f$ ) by

$$\pi_A = \sqrt{2} \sum_{k=1}^{N_f} (T_{k,k}^A \pi'_{k,k}) . \quad (2.15)$$

In this,  $T^A$  are the diagonal generators of the  $SU(N_f)$  group corresponding to  $\pi_A$ , expressed as

$$T_{k,j}^A = \frac{\delta_{k,j}}{\sqrt{2A(A+1)}} \times \begin{cases} 1 , & 1 \leq k < A+1 \\ -A , & k = A+1 \\ 0 , & A+1 < k \leq N_f \end{cases} , \quad A = 1, 2, \dots, N_f - 1 . \quad (2.16)$$

Equation (2.7) gives

$$\mathcal{L}_{\text{eff}} \supset -\frac{1}{2} \sum_{A,B=1}^{N_f-1} [M_\pi^2]_{A,B} \pi_A \pi_B , \quad (2.17)$$

where

$$[M_\pi^2]_{A,B} = 4B_0 \text{Tr} [T^A T^B M_q] . \quad (2.18)$$

Quark compositions and squared masses of dark mesons are summarized in Table 1. In the scenario where all dark quarks possess identical masses, i.e.,

$$m_k = m_q , \quad k = 1, 2, \dots, N_f , \quad (2.19)$$

all dark mesons will consequently exhibit the same mass, given by

$$M_{\pi'_{k,j}} = M_{\pi_A} = \sqrt{2B_0 m_q} , \quad k, j = 1, 2, \dots, N_f \text{ with } k \neq j , \quad A = 1, 2, \dots, N_f - 1 . \quad (2.20)$$

The parameters mentioned above are related approximately by

$$F_0 \sim \Lambda_{\text{dQCD}} , \quad (2.21)$$

$$N_f F_0^2 B_0 = -\langle \bar{q}q \rangle . \quad (2.22)$$

Thus, in the numerical calculations performed in this study, we choose  $F_0$ ,  $B_0$ , and the dark quark masses  $m_k$  ( $k = 1, 2, \dots, N_f$ ) as the fundamental parameters.

dark meson	quark composition	squared mass
$\pi'_{k,j}$ ( $k \neq j$ )	$i\bar{q}_k \gamma^5 q_j$	$M_{\pi'_{k,j}}^2 = B_0(m_k + m_j)$
$\pi_A$ ( $A = 1, 2, \dots, N_f - 1$ )	$i\sqrt{2} \sum_{k=1}^{N_f} \left( T_{k,k}^A \bar{q}_k \gamma^5 q_k \right)$	$[M_\pi^2]_{A,B} = 4B_0 \text{Tr} [T^A T^B M_q]$
$\eta_1$	$\frac{i}{\sqrt{N_f}} \sum_{k=1}^{N_f} (\bar{q}_k \gamma^5 q_k)$	

**Table 1:** Quark compositions and squared masses of dark mesons.

In Eq. (2.7), the covariant derivative is expressed as

$$D_\mu U = \partial_\mu + iU \cdot L_\mu - iR_\mu \cdot U \quad (2.23)$$

with

$$L_\mu = -g' Z'_\mu \text{diag} \left( Q'_{1,L}, Q'_{2,L}, \dots, Q'_{N_f,L} \right) , \quad (2.24)$$

$$R_\mu = -g' Z'_\mu \text{diag} \left( Q'_{1,R}, Q'_{2,R}, \dots, Q'_{N_f,R} \right) . \quad (2.25)$$

Then, the first term in Eq. (2.7) gives the interaction between dark mesons and the  $U(1)_D$  gauge boson, which contains

$$\begin{aligned} \mathcal{L}_{\text{eff}} \supset & g' F_0 Z'_\mu \sum_{A=1}^{N_f-1} \left( \sum_{k=1}^{N_f} T_{k,k}^A (Q'_{k,R} - Q'_{k,L}) \right) \partial^\mu \pi_A \\ & - \frac{i}{2} g' Z'_\mu \sum_{1 \leq k < j \leq N_f} (Q'_{k,L} + Q'_{k,R} - Q'_{j,L} - Q'_{j,R}) (\pi'_{j,k} \partial^\mu \pi'_{k,j} - \pi'_{k,j} \partial^\mu \pi'_{j,k}) . \end{aligned} \quad (2.26)$$

As a benchmark scenario for the following study, we assume  $N_f = 3$  dark quark flavors with nearly degenerate masses. This leads to a spectrum of dark mesons where the Kaon-like and Pion-like states are the lightest degrees of freedom, with masses determined by the chiral symmetry breaking scale and quark masses. Due to the near-degeneracy, the kinematic distributions of dark mesons produced via the decays of heavier resonances remain largely insensitive to the small mass splittings. Furthermore, we assume vector-like  $U(1)_D$  charges for the dark quarks, specifically setting  $Q'_{k,L} = Q'_{k,R} = 1$  for two flavors ( $k = 1, 2$ ) and  $Q'_{3,L} = Q'_{3,R} = -1$  for the third, ensuring a simplified yet phenomenologically rich portal structure. Under this assignment, the  $Z'$  boson specifically couples to four flavor-carrying dark mesons (the Kaon-like states  $\pi'_{13}$  and  $\pi'_{23}$ ), while the remaining mesons (five pion and eta-like mesons), including the pion-like states and diagonal etas, remain uncoupled to the  $Z'$  due to the vector-like nature of the interaction and the charge degeneracy of the first two flavors. In what follows, for simplicity,  $\pi_D$  shall denote a generic dark meson, while  $K_D$  is reserved exclusively for those that couple to the  $Z'$ .

### 3 From Quark to Meson: modified Quark Combination Model

In the previous section, we summarized the effective low-energy description of the light dark-meson spectrum and couplings. To compute fluxes and detector event rates, however, an event-level prescription is required to map the initially produced dark quark pair into a set of dark meson four-momenta. Since hadronization is intrinsically non-perturbative, we model this stage using an MQCM, implementing the QCM plus longitudinal phase space approximation (LPSA) procedure adopted in Ref. [3]. In this setup, the final-state multiplicity and kinematics are generated stochastically, fixed by energy-momentum conservation in the hadronization rest frame. The resulting events are subsequently boosted to the laboratory frame to serve as input for propagation and scattering-rate calculations.

In our setup, the dark quark pair is produced through the  $Z'$  mediation. The relevant energy scale for hadronization is the invariant mass of the dark-quark system,

$$\sqrt{s} \equiv m_{q_k \bar{q}_k} = \sqrt{(p_{q_k}^\mu + p_{\bar{q}_k}^\mu)^2}. \quad (3.1)$$

For an on-shell  $Z'$  production and decay, one simply has  $p_{Z'}^\mu = p_{q_k}^\mu + p_{\bar{q}_k}^\mu$ , implying  $\sqrt{s} = m_{Z'}$ . We generate the final-state momenta in the  $Z'$  rest frame and then boost the full event to the laboratory frame using the (off-shell)  $Z'$  kinematics determined in the production stage.

For concreteness, we denote the meson as  $\pi_D$  and assume all mesons have nearly degenerate mass  $m_{\pi_D}$ . Following Ref. [3], we introduce the constituent-mass parameter entering the MQCM multiplicity ansatz,

$$m_{q_k} = \frac{m_{\pi_D}}{2}, \quad (3.2)$$

which acts as a phenomenological parameter internal to the hadronization model.

Within the quark-combination picture, the total number of dark mesons produced in an event,  $N$ , is assumed to obey a shifted-Poisson law:

$$P(N) = \frac{\langle N \rangle^{N-1}}{(N-1)!} e^{-\langle N \rangle}, \quad (3.3)$$

where the shift by 1 accounts for the original  $q_k \bar{q}_k$  pair. The average meson multiplicity is parameterized as [3]:

$$\langle N \rangle = \sqrt{\alpha^2 + \beta \sqrt{s}} - \alpha - 1, \quad \alpha = \beta m_{q_k} - \frac{1}{4}. \quad (3.4)$$

The parameter  $\beta$  governs the multiplicity scaling. For the SM QCD, the benchmark value  $\beta_{\text{BM}} = 4.2 \text{ GeV}^{-1}$ , derived from the QCM analysis of  $e^+ e^-$  data. To accommodate dark meson masses that may differ significantly from the QCD scale, we introduce a smooth interpolation for  $\beta$  dependent on the confinement scale  $\Lambda_D \equiv m_{\pi_D}$ :

$$\beta(\Lambda_D) = \beta_{\text{BM}} \left[ 1 + \left( \frac{1 \text{ GeV}}{\Lambda_D} \right)^p \right]^{1/p}. \quad (3.5)$$

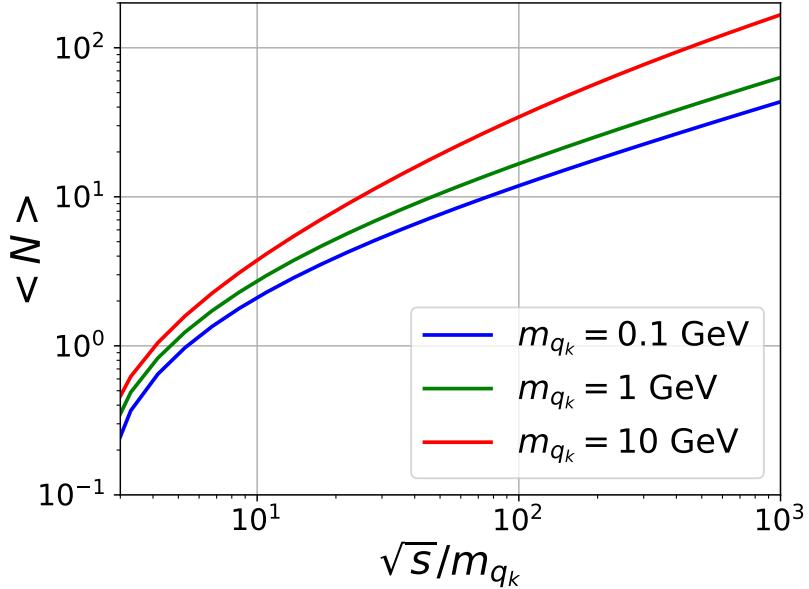


**Figure 1:** Average meson multiplicity  $\langle N \rangle$  as a function of the dimensionless scaled center-of-mass energy  $\sqrt{s}/m_{q_k}$ . The separation of curves indicates a violation of simple scaling, revealing the dependence of multiplicity on the absolute energy scale  $\sqrt{s}$  in addition to the kinematic ratio.

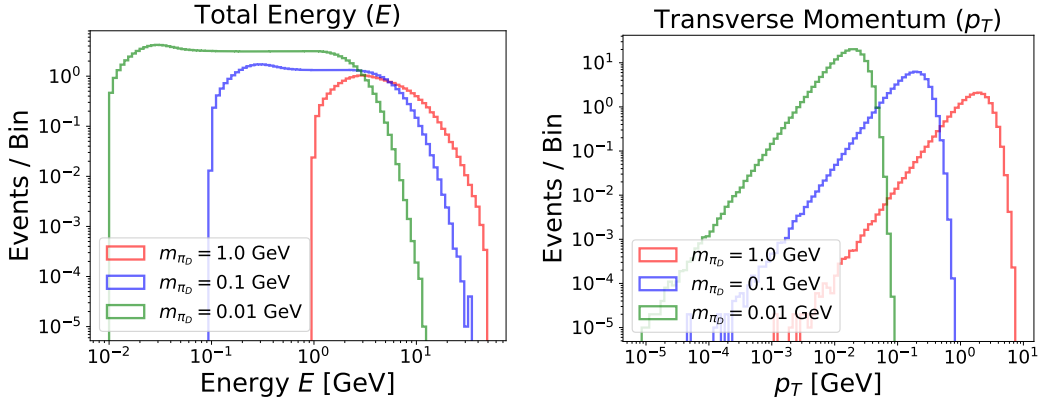
Numerical checks indicate that the final observables are largely insensitive to the precise value of the exponent  $p$ ; we therefore fix  $p = 2$  for simplicity. This ansatz ensures that for light dark sectors ( $\Lambda_D \ll \Lambda_{\text{QCD}}$ ), the multiplicity scales appropriately with the mass dimension.

Figure 1 illustrates the scaling behavior of the average meson multiplicity  $\langle N \rangle$  across different dark sector mass scales. As expected, the multiplicity grows consistently with the available phase space, scaling approximately linearly with the energy ratio  $\sqrt{s}/m_{q_k}$  in the log-log representation. However, a mild mass dependence is observed. For a fixed kinematic ratio  $\sqrt{s}/m_{q_k}$ , heavier dark sectors yield higher multiplicities compared to lighter sectors. This behavior reflects the interplay between the explicitly broken scale invariance of Eq. (3.5) and the dominant dependence of multiplicity on the absolute center-of-mass energy  $\sqrt{s}$ . Although the scaling of  $\beta(\Lambda_D)$  enhances the production efficiency for light sectors, it does not fully compensate for the reduced absolute energy  $\sqrt{s}$  at a fixed ratio  $\sqrt{s}/m_{q_k}$ . Moreover, the mass dependent feature also indicates that our estimation for  $\langle N \rangle$  is conservative for a model with sub-GeV DM scale.

To construct the four-momenta of the  $N$  dark mesons, we employ the LPSA procedure [3], which assumes approximately uniform rapidities within the kinematically allowed interval. We draw independent  $\xi_i \in [0, 1]$  and define

$$Y_i = Z + \xi_i Y \quad (i = 1, \dots, N), \quad (3.6)$$

where the auxiliary parameters  $Z$  and  $Y$  are fixed by energy-momentum conservation in



**Figure 2:** Kinematic distributions of the produced dark mesons in the  $q_k\bar{q}_k$  rest frame for a center-of-mass energy  $\sqrt{s} = 100$  GeV. The distributions are shown for three benchmark dark meson masses:  $m_{\pi_D} = 1.0$  GeV (red), 0.1 GeV (blue), and 0.01 GeV (green). Left: dark meson energy spectrum. Right: transverse momentum distribution of dark mesons.

the hadronization rest frame (*i.e.*  $q_k\bar{q}_k$  rest frame):

$$\sum_{i=1}^N E_i = \sqrt{s}, \quad \sum_{i=1}^N p_{L,i} = 0. \quad (3.7)$$

The transverse momenta are modeled with a Gaussian distribution subject to momentum conservation:

$$f(\vec{p}_{T,1}, \dots, \vec{p}_{T,N}) \propto \left[ \prod_{i=1}^N \exp\left(-\frac{\vec{p}_{T,i}^2}{\bar{\sigma}^2}\right) \right] \delta^{(2)}\left(\sum_{i=1}^N \vec{p}_{T,i}\right). \quad (3.8)$$

The width parameter  $\bar{\sigma}$  determines the characteristic transverse spread. In the SM sector, the reference width  $\bar{\sigma}_{\text{SM}} = 0.36$  GeV [71]. For the DM case, we assume the transverse kinematics scale linearly with the confinement energy to preserve the event shape topology. Identifying the confinement scale with the dark meson mass,  $\Lambda_D = m_{\pi_D}$ , we define the scaled width parameter as:

$$\bar{\sigma}(\Lambda_D) \equiv \bar{\sigma}_{\text{SM}} \frac{\Lambda_D}{\Lambda_{\text{QCD}}}, \quad (3.9)$$

where we adopt  $\Lambda_{\text{QCD}} = 0.25$  GeV as the conventional hadronic scale [71]. This scaling ensures that the jet-like structure of the DM events mimics QCD behavior but at a different mass scale.

The constructed meson energy and transverse momentum spectra for different masses with fixed  $\sqrt{s} = 100$  GeV are shown in Figure 2. In the left panel, the meson energy spectra show the shift towards lower energies for lighter sectors as the multiplicity increases. In the right panel, the spectral broadening for heavier masses reflects the linear scaling of the width parameter  $\bar{\sigma}$  with  $m_{\pi_D}$  defined in Eq. (3.9).

With the momenta generated in the center-of-mass frame, the kinematics of all dark mesons are fully determined. Each of the meson transverse mass is given by  $m_{T,i} =$

$\sqrt{m_{\pi_D}^2 + \vec{p}_{T,i}^2}$ , and the four-momentum in the hadronization rest frame is defined as  $p_i^{\mu,\text{rest}} = (E_i, \vec{p}_{T,i}, p_{L,i})$ . To interface with the laboratory frame production mechanism, we perform a Lorentz boost on the entire final state:  $p_i^{\mu,\text{lab}} = \Lambda^{\mu}_{\nu}(\beta_{Z'}) p_i^{\nu,\text{rest}}$ , where the boost vector  $\beta_{Z'}$  is determined by the (off-shell)  $Z'$  boson's four-momentum. The resulting set  $\{p_i^{\mu,\text{lab}}\}$  constitutes the dark-matter beam used for the subsequent flux convolution.

## 4 Productions of Dark Gauge Boson and Dark Meson

A comprehensive analysis of DM production channels in the upper atmosphere is central to the proposed search strategy. In this section, we detail the cross-section calculations for the three primary production mechanisms: proton bremsstrahlung, the decay of SM mesons, and the Drell-Yan process.

### 4.1 Proton Bremsstrahlung Production

We consider the production of a light vector boson  $Z'$  in cosmic-ray collisions via the bremsstrahlung-like process  $p + N \rightarrow p + N + Z'$ , where  $N$  denotes an atmospheric nucleon. For simplicity, we use the (total)  $pp$  scattering cross section  $\sigma_{pp}$  as an effective hadronic input to obtain an order-of-magnitude estimate.

In the laboratory frame, the incoming proton has energy  $E_p$  and three-momentum magnitude

$$P \equiv |\vec{p}_p| = \sqrt{E_p^2 - m_p^2}. \quad (4.1)$$

The emitted  $Z'$  is characterized by its laboratory energy  $E_{Z'}$  and transverse momentum  $p_T$ . Defining

$$p_{Z'} \equiv |\vec{p}_{Z'}| = \sqrt{E_{Z'}^2 - m_{Z'}^2}, \quad p_L = \sqrt{E_{Z'}^2 - m_{Z'}^2 - p_T^2}, \quad (4.2)$$

we introduce the longitudinal momentum fraction

$$z \equiv \frac{p_L}{P} = \frac{\sqrt{E_{Z'}^2 - m_{Z'}^2 - p_T^2}}{\sqrt{E_p^2 - m_p^2}}, \quad (4.3)$$

and the kinematic combination

$$H \equiv p_T^2 + (1 - z)m_{Z'}^2 + z^2m_p^2. \quad (4.4)$$

Following Ref. [72], we write the double-differential production cross section in variables  $(z, p_T^2)$  as

$$\frac{d^2\sigma_{\text{brem}}}{dz dp_T^2} = \sigma_{pp}(s') w_{ba}(z, p_T^2) |F_1(m_{Z'}^2)|^2, \quad (4.5)$$

where  $F_1$  is an effective nucleon electromagnetic form factor modeled using the vector-meson dominance prescription. The reduced invariant mass squared after radiating energy  $E_{Z'}$  is taken to be

$$s' \simeq 2m_p(E_p - E_{Z'} + m_p), \quad (4.6)$$

while the initial fixed-target invariant mass squared is

$$s = 2m_p(E_p + m_p) . \quad (4.7)$$

To obtain the spectrum in  $E_{Z'}$ , we transform from  $z$  to  $E_{Z'}$  at fixed  $p_T^2$  using Eq. (4.3). The corresponding Jacobian is

$$\left| \frac{\partial z}{\partial E_{Z'}} \right| = \frac{E_{Z'}}{z(E_p^2 - m_p^2)} , \quad (4.8)$$

so that

$$\frac{d^2\sigma_{\text{brem}}}{dE_{Z'} dp_T^2} = \sigma_{pp}(s') w_{ba}(z, p_T^2) \frac{E_{Z'}}{z(E_p^2 - m_p^2)} |F_1(m_{Z'}^2)|^2 . \quad (4.9)$$

We then define the *multiplicity per pp collision* as

$$\frac{d^2N_{\text{brem}}}{dE_{Z'} dp_T^2} \equiv \frac{1}{\sigma_{pp}(s)} \frac{d^2\sigma_{\text{brem}}}{dE_{Z'} dp_T^2} = \frac{\sigma_{pp}(s')}{\sigma_{pp}(s)} w_{ba}(z, p_T^2) \frac{E_{Z'}}{z(E_p^2 - m_p^2)} |F_1(m_{Z'}^2)|^2 , \quad (4.10)$$

where the splitting kernel for emission of a massive vector boson is

$$w_{ba}(z, p_T^2) = \frac{g_{\text{SM}}^2}{16\pi^2 H} \left[ 2 \frac{1 + (1 - z)^2}{z} - 4z(1 - z) \frac{2m_p^2 + m_{Z'}^2}{H} \right. \\ \left. + \frac{4z(1 - z)}{H^2} \left\{ z^2 m_p^4 + (1 - z) m_{Z'}^4 + (z^2 - 2z + 2) m_p^2 m_{Z'}^2 \right\} \right] . \quad (4.11)$$

To remain within the validity regime of the relativistic approximation used in Ref. [72], we impose the fixed numerical cuts  $E_p > 3m_p$ ,  $E_{Z'} > 3m_{Z'}$ , and  $p_T < (E_p - E_{Z'})/3$ . In addition, we apply the virtuality cut used there. The minimum virtuality of the exchanged photon is estimated as

$$|q_{\min}^2| \simeq \frac{z^2(1 - z)^2}{4E_p^2} H^2 . \quad (4.12)$$

We then require  $|q_{\min}^2| < \Lambda_{\text{QCD}}^2$  with  $\Lambda_{\text{QCD}} = 0.25$  GeV.

The total bremsstrahlung production cross section  $\sigma(pp \rightarrow ppZ')$  is obtained by integrating Eq. (4.9) over the allowed phase space, and is shown in the left panel of Fig. 3. Finally, we convolve the per-collision multiplicity with the isotropic cosmic-ray proton flux  $\phi_p(E_p)$  to obtain the differential  $Z'$  flux at the production point,

$$\Phi_{Z'}(E_{Z'}) = 2\pi \int_{E_{p,\min}}^{\infty} dE_p \phi_p(E_p) \int dp_T^2 \frac{d^2N_{\text{brem}}}{dE_{Z'} dp_T^2} , \quad (4.13)$$

where the prefactor  $2\pi$  corresponds to integrating an isotropic differential flux over the downward hemisphere. The resulting spectra are presented in the right panel of Fig. 3.

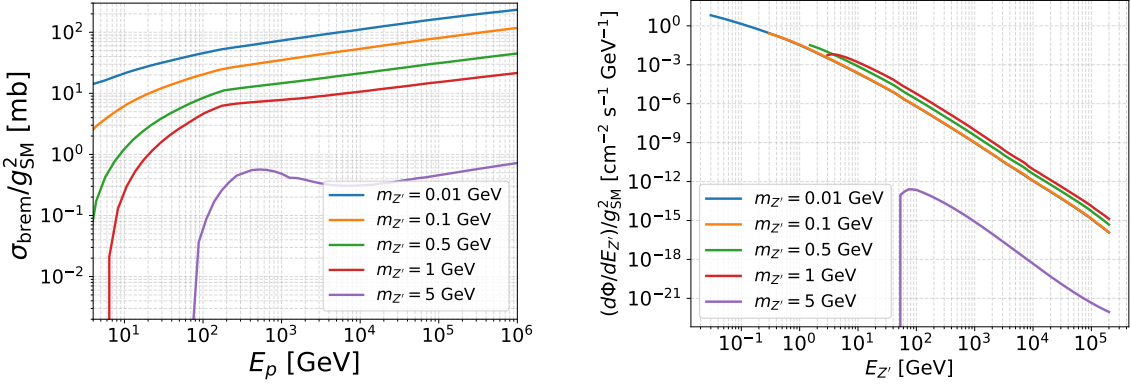


**Figure 3: Left:** The bremsstrahlung production cross-section  $\sigma(pp \rightarrow ppZ')$  as a function of the incident proton energy  $E_p$  for  $m_{Z'} = 0.01, 0.1, 0.5, 1.0, 5.0$  GeV, computed with the benchmark coupling  $g_{SM} = 1$  (to be rescaled when deriving limits). **Right:** The corresponding differential flux of  $Z'$  at the production point as a function of  $E_{Z'}$ , obtained from the multiplicity convolution in Eq. (4.13).

## 4.2 SM Meson Decay

Cosmic-ray proton interactions with atmospheric nuclei initiate hadronic cascades at energies exceeding a few GeV, producing copious amounts of pseudoscalar mesons, primarily  $\pi^0$  and  $\eta$ . In scenarios involving a light dark sector, these SM mesons serve as a potent source of dark gauge bosons ( $Z'$ ) via rare radiative decays, provided  $m_{Z'} < m_{\pi, \eta}$ . We focus on the mass hierarchy where the dark gauge boson is more than twice as heavy as the dark quarks ( $m_{Z'} > 2m_{q_k}$ ), such that the on-shell decay ( $Z' \rightarrow q_k \bar{q}_k$ ) dominates the production of dark sector particles.

The primary production channels for dark gauge bosons from pseudoscalar mesons are the radiative decays  $\pi^0 \rightarrow Z' \gamma$  and  $\eta \rightarrow Z' \gamma$ . The branching fractions for these processes, governed by the gauge coupling to the SM fermions and the phase space suppression, are given by:

$$\text{Br}(\pi^0 \rightarrow \gamma Z') = 2\epsilon^2 \left(1 - \frac{m_{Z'}^2}{m_{\pi^0}^2}\right)^3 \text{Br}(\pi^0 \rightarrow \gamma\gamma), \quad (4.14)$$

$$\text{Br}(\eta \rightarrow \gamma Z') = 2\epsilon^2 \left(1 - \frac{m_{Z'}^2}{m_\eta^2}\right)^3 \text{Br}(\eta \rightarrow \gamma\gamma), \quad (4.15)$$

where  $\epsilon = 3g_{SM}/e$ <sup>1</sup> in our setup, and the SM meson branching ratios are  $\text{Br}(\pi^0 \rightarrow \gamma\gamma) \sim 0.99$  and  $\text{Br}(\eta \rightarrow \gamma\gamma) \sim 0.39$  [73]. We assume that the dark photon subsequently decays into dark quarks with a branching ratio of  $\text{Br}(Z' \rightarrow q_k \bar{q}_k) \sim 1$ , which is valid when  $g_{SM}$  is

<sup>1</sup>The factor of 3 arises from the triangle anomaly. The amplitude for  $\pi^0 \rightarrow \gamma\gamma$  is proportional to  $(Q_u^{\text{EM}})^2 - (Q_d^{\text{EM}})^2 = 1/3$ , whereas the amplitude for  $\pi^0 \rightarrow \gamma Z'$  is proportional to  $Q_u^{\text{EM}} - Q_d^{\text{EM}} = 1$ , given that the up and down quarks are assumed to have the same coupling under  $U(1)_D$ . Similarly, the corresponding factor for the octet  $\eta$  state is also 3, though it is subject to a correction due to octet-singlet mixing. We will neglect this correction effect in our analysis.

small enough that decays to SM fermions are suppressed relative to the dark sector channel (assuming  $g' \gg g_{\text{SM}}$ ).

To model the production of atmospheric mesons, we adopt the calculation framework implemented in the HEAVENLYMCP code [48]. This tool incorporates the Matrix Cascade Equation (MCEq) package [74] to solve for the depth-dependent meson fluxes, utilizing the cosmic ray spectrum model from [75], the hadronic interaction model [76] and the atmospheric model [77]. While HEAVENLYMCP was originally designed to compute the flux of millicharged particles via the three-body decay of SM mesons, we have adapted the framework to instead simulate the two body radiative decays  $\pi^0 \rightarrow Z'\gamma/\eta \rightarrow Z'\gamma$ . The dark gauge boson fluxes for different mediator masses are presented in Figure 4.

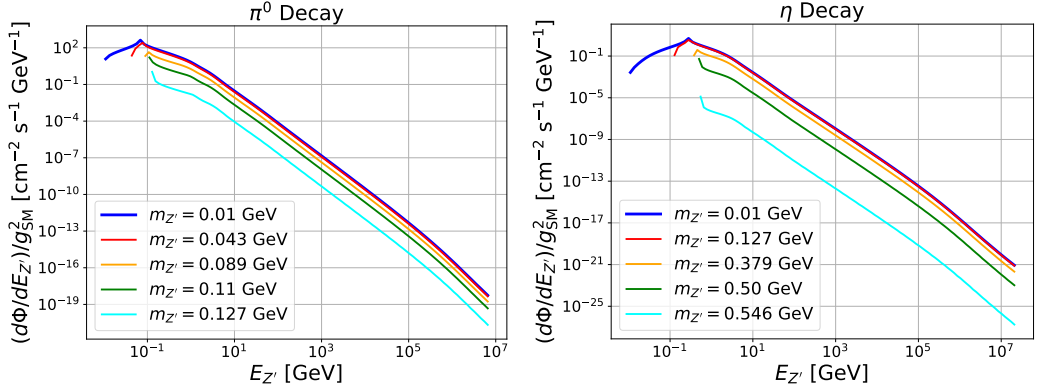


**Figure 4:**  $Z'$  Flux from  $\pi^0$  and  $\eta$  decay

Finally, the dark gauge boson flux is converted into a flux of dark pions via the hadronization process described in Section 3. Since the dark quarks are produced from the decay of an on-shell  $Z'$ , the center-of-mass energy for the hadronization process in the Modified Quark Combination Model is fixed at  $\sqrt{s} = m_{Z'}$ . The dark pion fluxes at the Earth's surface resulting from  $\pi^0$  and  $\eta$  decays are presented below in this section.

### 4.3 Drell-Yan Production of Dark Quark

Dark quarks can be produced via the  $s$ -channel exchange of a virtual  $Z'$  through quark-antiquark parton scattering,  $q\bar{q} \rightarrow Z'^* \rightarrow q_k\bar{q}_k$ . This Drell-Yan production process is particularly significant when the mass of the dark gauge boson is  $\gtrsim \mathcal{O}(1)$  GeV. We calculate the corresponding differential cross sections for dark quark pair production using `MadGraph5` [78], incorporating UFO model files generated by `FeynRules` [79]. In our simulation, the dark sector gauge coupling is set to unity, while the SM coupling  $g_{\text{SM}}$  is fixed at  $10^{-2}$ . This configuration reflects the parameter space of interest, characterized by  $g' \sim 1$  and  $g_{\text{SM}} \ll 1$ , where the width of the  $Z'$  is dominated by the decay channel  $Z' \rightarrow q_k\bar{q}_k$ . Reducing  $g_{\text{SM}}$  to a smaller value does not affect the kinematic distributions presented in this work, as it serves primarily as a normalization factor in this regime.

All events are simulated in the Laboratory frame, assuming a fixed-target configuration with one of the protons at rest. In Figure 5, we present the invariant mass distribution of the dark quark pair for various incident proton energies. It is observed that the differential

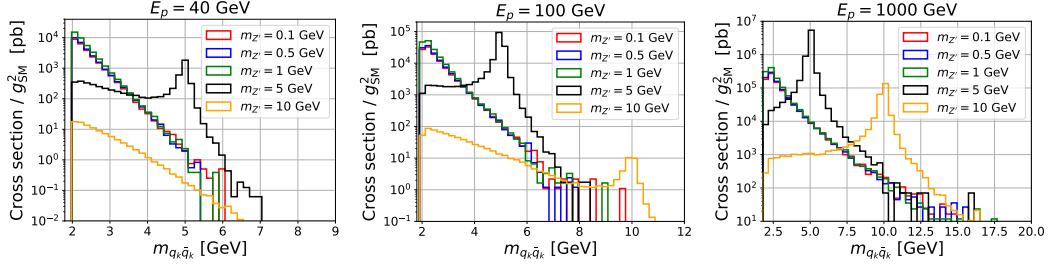


**Figure 5:** The differential production cross section of the Drell-Yan process for different incident proton energies ( $E_p$ ). From left to right,  $E_p = 40, 100$ , and  $1000$  GeV.

cross section exhibits a weak dependence on the  $Z'$  mass in the regime where  $m_{Z'} \lesssim \mathcal{O}(1)$  GeV. However, a significant resonant enhancement appears when the center-of-mass energy of the colliding protons,  $\sqrt{s} \sim \sqrt{2m_p E_p}$ , exceeds the  $Z'$  mass. This invariant mass peak becomes increasingly pronounced at higher collision energies, attributed to the reduced suppression from Parton Distribution Functions (PDFs) at the relevant momentum fractions. Specifically, for the lower incident energy of  $E_p = 40$  GeV, the production of heavier mediators (e.g.,  $m_{Z'} = 5, 10$  GeV) is kinematically forbidden or highly suppressed. As  $E_p$  increases to  $1000$  GeV, the resonance peaks for all considered masses become clearly distinguishable. Furthermore, in the low invariant mass region ( $m_{q_k\bar{q}_k} \ll m_{Z'}$ ), the cross section exhibits a continuum behavior dominated by off-shell exchange, which explains the overlapping curves for light  $Z'$  scenarios.

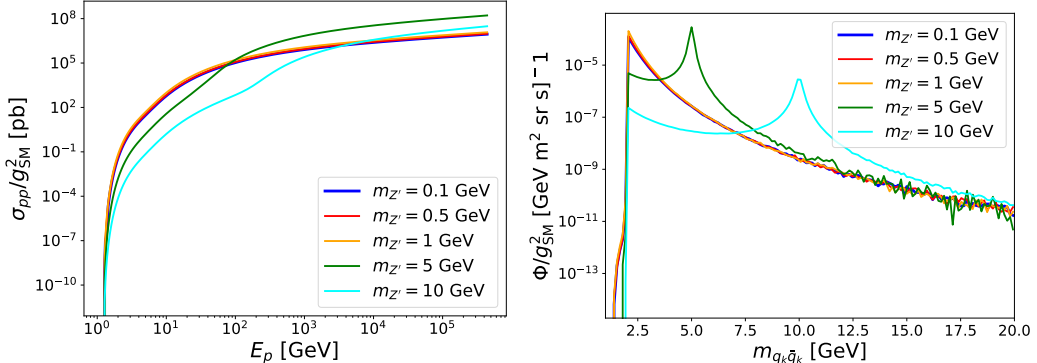


**Figure 6:** Left: Total production cross section of the Drell-Yan process as a function of incident proton energy. Right: The differential flux in terms of the dark quark pair invariant mass  $m_{q_k\bar{q}_k}$  due to the Drell-Yan process.

In the left panel of Figure 6, we illustrate the total cross section for the Drell-Yan process, normalized to unit couplings  $g_{\text{SM}} = 1$ . The dark matter gauge coupling  $g' = 1$ , and the mass of the  $Z'$  boson is indicated in the legend. While the dark quark mass is set to  $m_{Z'}/100$  in this simulation, we found that the total cross section is insensitive to the specific dark quark mass, provided it remains significantly lighter than the  $Z'$ . As indicated in the figure and consistent with the differential distributions in Figure 5, the total cross

sections are nearly identical for  $m_{Z'} \lesssim \mathcal{O}(1)$  GeV. For heavier  $Z'$  masses, the cross section drops sharply at lower proton energies where the center-of-mass energy is insufficient to produce the on-shell resonance. As the incident energy increases, the cross sections for different masses tend to converge and saturate. In this energy regime, the production rate is mainly governed by the couplings and the overall PDF scaling.

The differential flux from the Drell-Yan process is then straightforwardly obtained by convoluting the production cross section with the cosmic ray proton flux  $\phi_p(E_p)$ :

$$\Phi_{Z'}(m_{q_k \bar{q}_k}) = \int dE_p \phi_p(E_p) \frac{1}{\sigma_{pp}^{\text{tot}}(E_p)} \frac{d\sigma_{pp}^{\text{DY}}(E_p)}{dm_{q_k \bar{q}_k}} , \quad (4.16)$$

where  $\sigma_{pp}^{\text{tot}}(E_p)$  is the total proton-proton collision cross section, taken from the Particle Data Group [73]. The corresponding fluxes for different  $Z'$  masses are plotted in the right panel of Figure 6. Similar to the cross sections, the flux dependence on  $m_{Z'}$  is quite weak for  $m_{Z'} \lesssim \mathcal{O}(1)$  GeV. For heavier  $Z'$ , although the flux of high-energy cosmic ray protons is steeply falling, the resonance peak remains prominent. In fact, even after accounting for the power-law suppression of the cosmic ray spectrum, the dark quark pair flux is still dominated by production at the  $Z'$  mass pole for  $m_{Z'} = 5$  and 10 GeV.

#### 4.4 Overall Flux of Dark Meson

Sections 4.1-4.3 provide the differential partonic flux from the relevant atmospheric production mechanisms considered in this work. For a fixed mediator mass  $m_{Z'}$ , we construct the total partonic flux by summing the channel contributions at the level of the same laboratory-frame observable (here taken to be the  $Z'$  total energy  $E_{Z'}$ ). This total  $Z'$  flux <sup>2</sup> is the only production input needed for calculating the dark meson flux. Note that we assume the dark matter coupling  $g' \gg g_{\text{SM}}$ , so that the  $Z'$  dominantly decays into the dark quark pair.

Given  $(m_{q_k \bar{q}_k}, m_{\pi_D})$ , we then apply the event-level prescription of Section 3 to map each produced partonic configuration into a set of final-state dark-meson four-momenta, and thereby obtain the dark-meson energy spectrum. Since we assume nearly degenerate dark quark masses, different meson species should be produced with a similar amount and kinematics. Among all nine meson states, four of them will be interacting with SM particles through the  $Z'$  portal. So a factor of 4/9 is imposed when producing the meson flux. In what follows, we use  $E_{K_D}$  to denote the *total* energy of a single dark meson  $K_D$  in the laboratory frame. The resulting observable is the differential flux  $d\Phi/dE_{K_D}$ , reported throughout normalized by  $g_{\text{SM}}^2$  so that alternative coupling choices can be obtained by a simple rescaling.

Figure 7 summarizes the final output of this pipeline. The left panel shows the energy-integrated dark-Kaon ( $K_D$ ) flux as a function of  $m_{Z'}$ , where the integration is performed over  $E_{K_D}$  for the chosen benchmark value of  $m_{Z'} = 100m_{q_k}$  and  $m_{\pi_D} = 2m_{q_k}$ . The decomposition highlights how the relative importance of the individual  $Z'$  production mechanisms

---

<sup>2</sup>An off-shell  $Z'^*$  is referred to for the Drell-Yan production channel.

propagates into the final  $K_D$  yield once the hadronization mapping is applied. In particular, the meson-decay contributions exhibit the expected kinematic shutoff once  $m_{Z'}$  exceeds the parent-meson mass, while the remaining channels continue to contribute at larger  $m_{Z'}$ .

The right panel displays the differential energy spectrum  $(d\Phi/dE_{K_D})/g_{\text{SM}}^2$  for a representative benchmark  $m_{Z'} = 0.1$  GeV. The overall spectral falloff follows from the steeply decreasing cosmic-ray spectrum encoded in the parent  $Z'$  flux, while the detailed shape and the relative channel weights reflect the interplay between the production kinematics of different channels and the hadronization/fragmentation pattern. This  $E_{K_D}$ -differential flux will be used as the input for the detector-level scattering calculations in the next section.

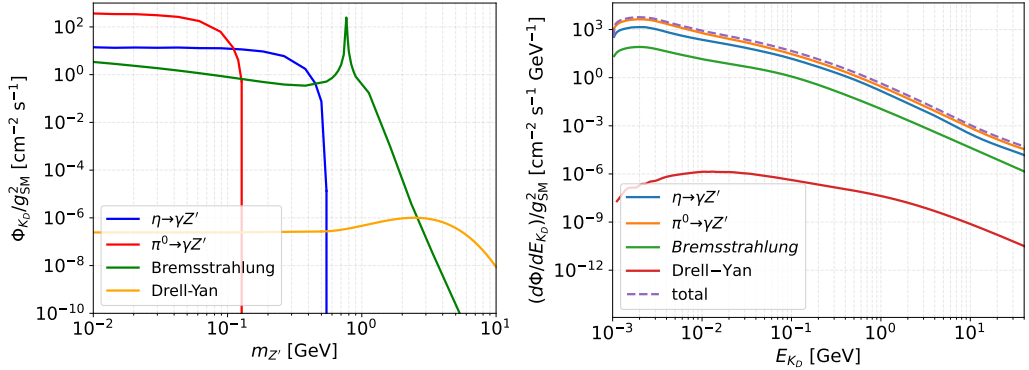


**Figure 7:** Left: energy-integrated dark-meson flux (integrated over  $E_{K_D}$ ) as a function of the mediator mass  $m_{Z'}$ , shown decomposed into the contributions associated with the individual production mechanisms and normalized by  $g_{\text{SM}}^2$ . Right: differential dark-meson energy spectrum  $(d\Phi/dE_{K_D})/g_{\text{SM}}^2$  for  $m_{Z'} = 0.1$  GeV.

## 5 DM-Nucleus Scattering at The JUNO Detector

As discussed in Section 2, the 4/9 of the dark meson species, denoted by  $K_D$ , interacts with the SM via a vector mediator  $Z'$ . In our simulation, we adopt the scalar DM tune within GENIE, where the DM particle is a complex scalar coupled to a vector mediator. The interaction Lagrangian describing the coupling of the mediator to the DM and SM fermions in accordance with the definition in GENIE is given by:

$$\mathcal{L}_{\text{int}} = 2 \times ig' Z'^\mu (K_D^* \partial_\mu K_D - \partial_\mu K_D^* K_D) + g_{\text{SM}} Z'_\mu \sum_f \bar{\psi}_f \gamma^\mu (Q_L^f P_L + Q_R^f P_R) \psi_f , \quad (5.1)$$

where  $f/K_D$  denotes the SM fermions / Kaon-like dark mesons,  $P_{L,R}$  are the chiral projection operators, and the factor of 2 entering the  $K_D$  coupling originates from the charge assignment defined in Eq. 2.26. We assume vector-like couplings to the SM fermions such that  $Q_L^f = Q_R^f = Q_V^f$ .

### 5.1 Simulation Framework with GENIE

Hadronic interactions of DM share significant kinematic and dynamical similarities with neutral-current (NC) neutrino scattering. Consequently, it is natural to utilize established

neutrino Monte Carlo software suites for simulations. We employ the **GENIE** generator [69, 70], specifically integrating the Boosted Dark Matter (BDM) module [67] to perform cross-section calculations and event generation.

GENIE provides a comprehensive simulation of nuclear effects, including nucleon Fermi motion, Pauli blocking, and Final-State interactions of hadrons as they exit the nuclear remnant. The simulation covers two primary scattering regimes:

1. **Elastic Scattering (EL):** The DM undergoes elastic scattering off nucleons. Under the assumption of a vector coupling, the process is described by the nucleon vector form factors ( $F_1$  and  $F_2$ ), which parameterize the charge and magnetic moment distributions. Consistent with the implementation in GENIE, these form factors are assumed to have a dipole form. Their normalizations are constrained by the nucleon electric charges and anomalous magnetic moments.
2. **Deep Inelastic Scattering (DIS):** For high momentum transfer, the interaction enters the Deep Inelastic Scattering (DIS) regime. In the case of complex scalar dark matter with a vector coupling, the scattering cross-section is described by a hadronic tensor dependent primarily on the  $F_1$  and  $F_2$  structure functions derived from parton distribution functions (PDFs). To extend validity into the relatively low- $Q^2$  regime characteristic of BDM scenarios, GENIE employs PDFs augmented with Bodek-Yang corrections. The hadronization of the final state is governed by the AGKY model, which selects the fragmentation scheme based on the invariant mass of the hadronic system ( $W$ ). For low  $W \lesssim 2.3$  GeV, an empirical KNO-based model tuned to neutrino data is utilized, while for high  $W \gtrsim 3$  GeV, the simulation transitions to PYTHIA fragmentation, with a linear transition window in between.

## 5.2 Cross-Section Calculation and Event Generation

The simulation workflow consists of two primary stages: the pre-computation of cross-section splines and the subsequent generation of scattering events.

First, we generate the scattering cross-section splines using the GENIE `gmkspl_dm` application. This step pre-calculates the interaction probabilities for the specific target nucleus. For the JUNO detector, the primary targets are  $^{12}\text{C}$  and  $^1\text{H}$ . We employ the `GDM18_00b_00_000` tune, which defines the physics model for scalar dark matter interactions. In this simulation, both the DM and SM couplings are normalized to unity, and the *gsm* will be rescaled subsequently to derive the sensitivity limits. We scan the dark gauge boson ( $Z'$ ) mass across the range of 1 MeV to 10 GeV, with the dark meson mass fixed at 1/50th of the  $Z'$  mass. This mass relation is consistent with the configuration used for the flux calculation in the preceding section. The splines are generated up to a maximum incident energy of  $E_{\text{max}} = 1000$  GeV with 200 knots per spline to ensure high-precision interpolation.

Utilizing the pre-computed cross section splines, event samples are generated via the GENIE `gevgen_dm` application. To characterize the differential cross-sections across a wide kinematic range, event simulations are performed at discrete incident DM kinetic energies. The energy points are sampled on a logarithmic scale up to 1 TeV. The lower energy

thresholds are set to 0.05 GeV for EL and 0.5 GeV for DIS. Flux contributions below these limits were found to yield negligible signal rates, mainly attributed to the suppressed scattering cross section and the signal selection cuts.

For a specific energy point  $E$ , the generation procedure is as follows:

```
gevgen_dm -n 10000 -m [Dark_Meson_Mass] -g 1 -z 100 -t [Target_PDG] \
--tune GDM18_00b_00_000 --event-generator-list [Channel] \
--cross-sections [Spline_File].xml \
-e $E --seed [Random_Seed] -o dm_[Channel]_E${E}.ghep.root
```

Here,  $-n$  sets the number of events to  $10^4$  to ensure sufficient statistics for event counting, and  $-t$  specifies the target nucleus code (e.g., 1000060120 for Carbon-12 in JUNO). The  $--event-generator-list$  flag is used to select between DMEL and DMDIS, allowing for the isolation of specific interaction channels. The output is saved in the native GHEP ROOT format and subsequently converted to the `gxml` summary format using the `gntp` utility for analysis.

### 5.3 Signal Selection and Sensitivity at JUNO

The total expected signal yield in the JUNO detector,  $N_{\text{total}}$ , is obtained by integrating the product of the flux and the scattering cross section over the incoming dark meson energy  $E_{K_D}$ :

$$N_{\text{total}} = T \times \int_{E_{\text{min}}}^{E_{\text{max}}} \frac{d\Phi}{dE_{K_D}} \times [N_{\text{H}} \cdot \sigma_{\text{H}}^{\text{vis}}(E_{K_D}) + N_{\text{C}} \cdot \sigma_{\text{C}}^{\text{vis}}(E_{K_D})] dE_{K_D} . \quad (5.2)$$

Here,  $T$  denotes the experimental exposure time (assumed to be 1 year), and  $d\Phi/dE_{k_D}$  represents the differential flux of the dark meson. The terms  $N_{\text{H}}$  and  $N_{\text{C}}$  correspond to the number of target Hydrogen and Carbon-12 nuclei contained within the 20 kton fiducial mass of JUNO, respectively. The quantities  $\sigma_{\text{H}}^{\text{vis}}(E_{K_D})$  and  $\sigma_{\text{C}}^{\text{vis}}(E_{K_D})$  denote the effective “visible” scattering cross-sections. These terms incorporate the detector response by accounting for the quenching effects on nuclear recoils<sup>3</sup> and enforcing an analysis threshold. As the JUNO detector is a large liquid scintillator detector, the signal consists of the visible energy deposited by the recoil products. We consider all visible final-state particles, including  $\mu^{\pm}, \pi^{\pm}, p, e^{\pm}$ , and  $\gamma$ , imposing a visible energy threshold of  $T_{\text{vis}} > 0.3$  MeV [81] as the selection criterion for signal candidates.

Table 2 summarizes the expected JUNO event yields for representative  $Z'$  masses under different visible-energy threshold assumptions (including a more stringent  $T_{\text{vis}}$  cut for reference), with the coupling fixed at  $g_{\text{SM}} = 10^{-3}$ . Two key trends are evident: (i) the yield increases rapidly as  $m_{Z'}$  decreases, reflecting the interaction rate enhancement associated with a lighter mediator; and (ii) raising the detection threshold from  $T_{\text{vis}} = 0.3$  MeV to 3 MeV reduces the acceptance, particularly for the elastic scattering on hydrogen in the lighter mediator regime. Across the considered benchmarks, elastic scattering on carbon consistently dominates the total yield, whereas the DIS contributions remain subleading.

---

<sup>3</sup>For recoil protons, we account for the non-linear light yield (quenching effect) utilizing the Birks’ law formulation described in Ref. [80].

Channel	$T_{\text{vis}} = 0.3 \text{ MeV}$			$T_{\text{vis}} = 3 \text{ MeV}$		
	0.1	0.01	0.001	0.1	0.01	0.001
	$(m_{Z'} \text{ in GeV})$			$(m_{Z'} \text{ in GeV})$		
Elastic ( $^{12}\text{C}$ )	4.06	$6.28 \times 10^2$	$1.13 \times 10^3$	2.92	$3.90 \times 10^2$	$7.02 \times 10^2$
Elastic (H)	2.27	$7.55 \times 10^1$	$8.18 \times 10^1$	0.739	9.08	9.90
Inelastic ( $^{12}\text{C}$ )	$4.81 \times 10^{-2}$	$8.33 \times 10^{-1}$	1.05	$4.79 \times 10^{-2}$	$8.28 \times 10^{-1}$	1.04
Inelastic (H)	$6.55 \times 10^{-3}$	$1.10 \times 10^{-1}$	$1.36 \times 10^{-1}$	$6.52 \times 10^{-3}$	$1.09 \times 10^{-1}$	$1.35 \times 10^{-1}$

**Table 2:** Predicted event counts for different  $Z'$  masses and detection energy thresholds ( $T_{\text{vis}}$ ). The Standard Model coupling is fixed at  $g_{\text{SM}} = 10^{-3}$  for reference. “Elastic (H/ $^{12}\text{C}$ )” and “Inelastic (H/ $^{12}\text{C}$ )” refer to elastic and deep inelastic scattering on Hydrogen/Carbon, respectively.

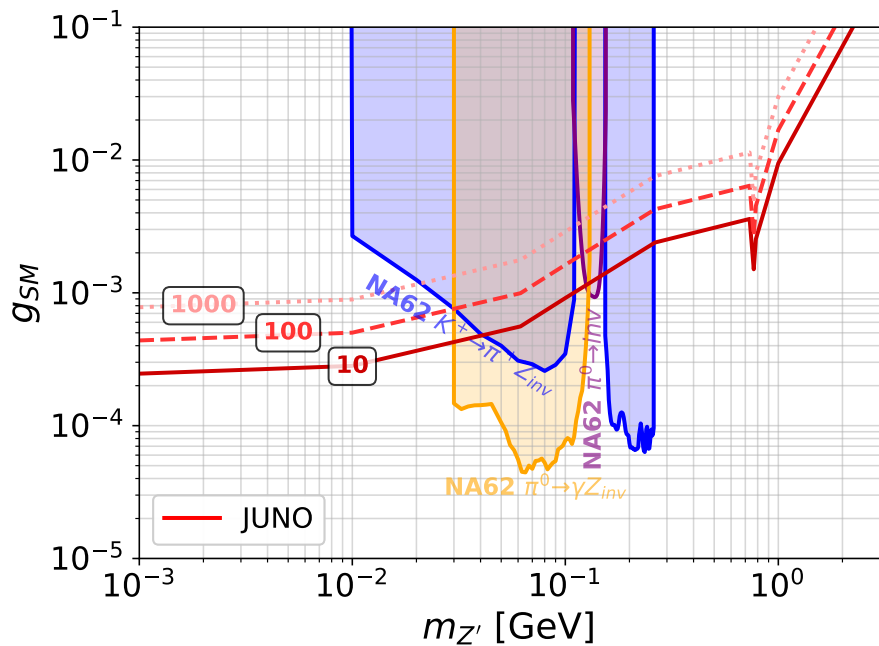


**Figure 8:** Projected sensitivity to the Standard Model coupling  $g_{\text{SM}}$  as a function of the  $Z'$  mass  $m_{Z'}$  at JUNO. The red contours represent the coupling strength required to observe 10 (solid), 100 (dashed), and 1000 (dotted) signal events, assuming a 1-year exposure. The shaded regions denote the parameter space currently excluded by NA62 constraints [82, 83].

The dominant background for energetic dark matter scattering in JUNO arises from neutral current interactions of atmospheric neutrinos [84–87]. While a detailed background subtraction analysis is beyond the scope of this work, we present signal yield contours to demonstrate the physics potential of the JUNO detector. The Figure 8 translates the predicted event yields into a sensitivity reach in the  $(m_{Z'}, g_{SM})$  plane. The projection assumes a 20 kton liquid-scintillator fiducial mass with a 1-year data-taking period. We combine the event yields from both carbon and hydrogen targets, adopting a carbon-to-hydrogen mass fraction of 88:12 [65].

The red contours depict the coupling required to accumulate a fixed number of signal events (10, 100, and 1000). Quantitatively, for light mediator ( $m_{Z'} \lesssim 10$  MeV), JUNO is sensitive to couplings as low as  $g_{SM} \sim 2.4 \times 10^{-4}$  (assuming a 10-event threshold). As the mediator mass increases to 100 MeV and 1 GeV, the coupling required for detection rises to approximately  $10^{-3}$  and  $10^{-2}$ , respectively. This reduced sensitivity arises from the interplay between flux suppression and the kinematic suppression of the scattering cross section. The shaded regions highlight existing exclusion limits from the NA62 experiment. The upper mass boundary of the NA62 exclusion is determined kinematically by the mass difference between the kaon and pion, while the lower mass boundary is constrained primarily by significant missing photon backgrounds in the low missing invariant mass region. Notably, the JUNO sensitivities are not only complementary to existing constraints in the mass windows of  $m_{Z'} < 10$  MeV and  $m_{Z'} > 0.26$  GeV, but are also projected to be more stringent than current NA62 limit for  $m_{Z'} \gtrsim 10$  MeV. This indicates that JUNO has the potential to probe a substantial region of parameter space for light dark mediators that currently remains unexplored.

## 6 Conclusions

In this work, we have presented a comprehensive study on the atmospheric production and terrestrial detection of sub-GeV dark mesons within the framework of a confining dark sector coupled to the SM via a leptophobic  $U(1)_D$  vector portal. By leveraging the high flux of cosmic rays and the large fiducial mass of the JUNO detector, we explored the sensitivity to light dark matter candidates which remain challenging to probe at collider experiments.

In the literature, the transition from dark quarks to dark mesons is often implemented using phenomenological models that are struggling to extrapolate to confinement scales far from that of the SM QCD. To address this, we implemented a modified Quark Combination Model to describe the non-perturbative dark hadronization process. We generalized the existing QCM to accommodate vastly varying dark confinement scales. In our setup, we observe that for a fixed kinematic ratio  $\sqrt{s}/m_{q_k}$ , a heavier dark sector scale yields higher meson multiplicities. The momenta of the final-state mesons are reconstructed via Monte-Carlo simulation utilizing the longitudinal phase space approximation.

We evaluate the atmospheric dark meson flux arising from three distinct production mechanisms: proton bremsstrahlung, SM meson decay ( $\pi^0, \eta \rightarrow \gamma Z'$ ), and Drell-Yan processes. Our analysis of the flux composition demonstrates that radiative decays of light

pseudoscalar mesons dominate the production in the low-mass mediator regime  $m_{Z'} \lesssim m_\eta$ , providing a potent source of light dark matter. As for heavier mediators ( $m_{Z'} \gtrsim 1$  GeV), the Drell-Yan process becomes the primary production channel, despite the steep fall-off of the cosmic ray spectrum.

Utilizing the GENIE generator with a customized BDM module, we simulate the interaction of relativistic dark mesons with the liquid scintillator target. We examined both elastic scattering and deep inelastic scattering channels on Carbon and Hydrogen nuclei. Our results indicate that the elastic scattering on Carbon is the dominant signal channel across most of the considered parameter space. Furthermore, we investigated the impact of detector thresholds. Raising the visible energy cut from 0.3 MeV to 3 MeV suppresses the total signal rate by a factor  $\sim 2$ . The reduction in signal acceptance for the Hydrogen scattering channel in the light mediator regime is most significant because of the softer recoil spectra.

Based on a projected 20 kton·year exposure, we derived exclusion limits on the SM coupling strength  $g_{\text{SM}}$ . JUNO exhibits strong sensitivity in the light mediator region ( $m_{Z'} \lesssim 10$  MeV), capable of probing coupling as low as  $g_{\text{SM}} \sim 2.4 \times 10^{-4}$ . Our analysis shows that JUNO provides constraints that are highly complementary to existing limits from the NA62 experiment. While NA62 is limited by kinematic thresholds and specific background windows, JUNO is sensitive to the unconstrained parameter space in the regions  $m_{Z'} \lesssim 10$  MeV and  $m_{Z'} \gtrsim 0.26$  GeV. Moreover, for  $m_{Z'} \gtrsim 10$  MeV, JUNO's projected limits are more stringent than current NA62 bounds.

## Acknowledgments

This work was supported by the Natural Science Foundation of Sichuan Province under grant No. 2026NSFSC0034, by the National Natural Science Foundation of China (Project NO. 11905149, 12505121), by the Joint Fund of Henan Province Science and Technology R&D Program (Project NO. 245200810077), and by the Startup Research Fund of Henan Academy of Sciences (Project NO. 20251820001).

## References

- [1] M. Battaglieri et al., *US Cosmic Visions: New Ideas in Dark Matter 2017: Community Report*, in *U.S. Cosmic Visions: New Ideas in Dark Matter*, 7, 2017 [[1707.04591](#)].
- [2] M.J. Strassler and K.M. Zurek, *Echoes of a hidden valley at hadron colliders*, *Phys. Lett. B* **651** (2007) 374 [[hep-ph/0604261](#)].
- [3] T. Han, Z. Si, K.M. Zurek and M.J. Strassler, *Phenomenology of hidden valleys at hadron colliders*, *JHEP* **07** (2008) 008 [[0712.2041](#)].
- [4] G.D. Kribs and E.T. Neil, *Review of strongly-coupled composite dark matter models and lattice simulations*, *Int. J. Mod. Phys. A* **31** (2016) 1643004 [[1604.04627](#)].
- [5] S. Gori et al., *Dark Sector Physics at High-Intensity Experiments*, [2209.04671](#).
- [6] Y. Bai and R.J. Hill, *Weakly Interacting Stable Pions*, *Phys. Rev. D* **82** (2010) 111701 [[1005.0008](#)].

- [7] M.R. Buckley and E.T. Neil, *Thermal Dark Matter from a Confining Sector*, *Phys. Rev. D* **87** (2013) 043510 [[1209.6054](#)].
- [8] J.M. Cline, Z. Liu, G.D. Moore and W. Xue, *Composite strongly interacting dark matter*, *Phys. Rev. D* **90** (2014) 015023 [[1312.3325](#)].
- [9] K. Harigaya and Y. Nomura, *Light Chiral Dark Sector*, *Phys. Rev. D* **94** (2016) 035013 [[1603.03430](#)].
- [10] S. Alexander, H. Gilmer, T. Manton and E. McDonough,  *$\pi$ -axion and  $\pi$ -axiverse of dark QCD*, *Phys. Rev. D* **108** (2023) 123014 [[2304.11176](#)].
- [11] Y. Chung, *Two coincidences are a clue: Probing a GeV-scale dark QCD sector*, [2506.10928](#).
- [12] Y. Hochberg, E. Kuflik, T. Volansky and J.G. Wacker, *Mechanism for Thermal Relic Dark Matter of Strongly Interacting Massive Particles*, *Phys. Rev. Lett.* **113** (2014) 171301 [[1402.5143](#)].
- [13] Y. Hochberg, E. Kuflik, H. Murayama, T. Volansky and J.G. Wacker, *Model for Thermal Relic Dark Matter of Strongly Interacting Massive Particles*, *Phys. Rev. Lett.* **115** (2015) 021301 [[1411.3727](#)].
- [14] H.M. Lee and M.-S. Seo, *Communication with SIMP dark mesons via  $Z'$ -portal*, *Phys. Lett. B* **748** (2015) 316 [[1504.00745](#)].
- [15] Y. Hochberg, E. Kuflik and H. Murayama, *SIMP Spectroscopy*, *JHEP* **05** (2016) 090 [[1512.07917](#)].
- [16] J.S. Bullock and M. Boylan-Kolchin, *Small-Scale Challenges to the  $\Lambda$ CDM Paradigm*, *Ann. Rev. Astron. Astrophys.* **55** (2017) 343 [[1707.04256](#)].
- [17] S. Tulin and H.-B. Yu, *Dark Matter Self-interactions and Small Scale Structure*, *Phys. Rept.* **730** (2018) 1 [[1705.02358](#)].
- [18] B. Holdom, *Two  $U(1)$ 's and Epsilon Charge Shifts*, *Phys. Lett. B* **166** (1986) 196.
- [19] R. Foot and X.-G. He, *Comment on  $Z$   $Z$ -prime mixing in extended gauge theories*, *Phys. Lett. B* **267** (1991) 509.
- [20] H.-C. Cheng, L. Li and E. Salvioni, *A theory of dark pions*, *JHEP* **01** (2022) 122 [[2110.10691](#)].
- [21] S. Born, R. Karur, S. Knapen and J. Shelton, *Scouting for dark showers at CMS and LHCb*, *Phys. Rev. D* **108** (2023) 035034 [[2303.04167](#)].
- [22] H.-C. Cheng, X.-H. Jiang, L. Li and E. Salvioni, *Dark showers from  $Z$ -dark  $Z'$  mixing*, *JHEP* **04** (2024) 081 [[2401.08785](#)].
- [23] H.-C. Cheng, X.-H. Jiang and L. Li, *Phenomenology of electroweak portal dark showers: high energy direct probes and low energy complementarity*, *JHEP* **01** (2025) 149 [[2408.13304](#)].
- [24] S. Liebersbach, P. Sandick, A. Shiferaw and Y. Zhao, *Exploring the hidden valley at MATHUSLA*, *Nucl. Phys. B* **1018** (2025) 117050 [[2408.07756](#)].
- [25] W. Liu, J. Lockyer and S. Kulkarni, *Hidden valley scenario sensitivity in the CMS muon end cap detector*, *Phys. Rev. D* **112** (2025) 075029 [[2505.03058](#)].
- [26] CMS Collaboration, *Search for low-mass hidden valley dark showers with displaced dimuons in proton-proton collisions at  $\sqrt{s} = 13$  TeV*, .

[27] E. Bernreuther, N. Hemme, F. Kahlhoefer, S. Kulkarni and M. Ovchynnikov, *Sub-GeV dark matter and multi-decay signatures from dark showers at beam-dump experiments*, [2510.23696](#).

[28] T. Cohen, M. Lisanti and H.K. Lou, *Semivisible Jets: Dark Matter Undercover at the LHC*, *Phys. Rev. Lett.* **115** (2015) 171804 [[1503.00009](#)].

[29] H. Beauchesne, E. Bertuzzo, G. Grilli Di Cortona and Z. Tabrizi, *Collider phenomenology of Hidden Valley mediators of spin 0 or 1/2 with semivisible jets*, *JHEP* **08** (2018) 030 [[1712.07160](#)].

[30] CMS Collaboration, *Search for resonant production of strongly coupled dark matter in proton-proton collisions at 13 TeV*, *JHEP* **06** (2022) 156 [[2112.11125](#)].

[31] B. Liu and K. Pedro, *Semi-visible jets + X: illuminating dark showers with radiation*, *JHEP* **12** (2024) 105 [[2409.04741](#)].

[32] A. Buckley, J. Butterworth, L. Corpe, C. Doglioni, D. Kar, C. Prat et al., *Probing the sensitivity of semi-visible jets to current LHC measurements using the CONTUR toolkit*, [2502.11237](#).

[33] ATLAS Collaboration, *Search for new physics in final states with semivisible jets or anomalous signatures using the ATLAS detector*, *Phys. Rev. D* **112** (2025) 012021 [[2505.01634](#)].

[34] P. Schwaller, D. Stolarski and A. Weiler, *Emerging Jets*, *JHEP* **05** (2015) 059 [[1502.05409](#)].

[35] CMS Collaboration, *Search for new particles decaying to a jet and an emerging jet*, *JHEP* **02** (2019) 179 [[1810.10069](#)].

[36] J. Carrasco and J. Zurita, *Emerging jet probes of strongly interacting dark sectors*, *JHEP* **01** (2024) 034 [[2307.04847](#)].

[37] ATLAS Collaboration, *Search for emerging jets in pp collisions at  $\sqrt{s} = 13$  TeV with the ATLAS experiment*, [2510.12347](#).

[38] J. Carrasco, S. Kulkarni, W. Liu, J. Lockyer and J. Zurita, *Semi-visible emerging jets*, [2511.02918](#).

[39] A. Kusenko, S. Pascoli and D. Semikoz, *New bounds on MeV sterile neutrinos based on the accelerator and Super-Kamiokande results*, *JHEP* **11** (2005) 028 [[hep-ph/0405198](#)].

[40] P.-f. Yin and S.-h. Zhu, *Detecting light long-lived particle produced by cosmic ray*, *Phys. Lett. B* **685** (2010) 128 [[0911.3338](#)].

[41] C. Argüelles, P. Coloma, P. Hernández and V. Muñoz, *Searches for Atmospheric Long-Lived Particles*, *JHEP* **02** (2020) 190 [[1910.12839](#)].

[42] P. Coloma, P. Hernández, V. Muñoz and I.M. Shoemaker, *New constraints on Heavy Neutral Leptons from Super-Kamiokande data*, *Eur. Phys. J. C* **80** (2020) 235 [[1911.09129](#)].

[43] J. Alvey, M. Campos, M. Fairbairn and T. You, *Detecting Light Dark Matter via Inelastic Cosmic Ray Collisions*, *Phys. Rev. Lett.* **123** (2019) 261802 [[1905.05776](#)].

[44] L. Su, W. Wang, L. Wu, J.M. Yang and B. Zhu, *Atmospheric Dark Matter and Xenon1T Excess*, *Phys. Rev. D* **102** (2020) 115028 [[2006.11837](#)].

[45] S. Airen, Z. Chacko, C. Kilic and R.P.R. Sudha, *Searching for hidden sector particles at neutrino telescopes*, *Phys. Rev. D* **112** (2025) 095044 [[2506.05326](#)].

[46] P.-K. Hu, A. Kusenko and V. Takhistov, *Dark Cosmic Rays*, *Phys. Lett. B* **768** (2017) 18 [[1611.04599](#)].

[47] R. Plestid, V. Takhistov, Y.-D. Tsai, T. Bringmann, A. Kusenko and M. Pospelov, *New Constraints on Millicharged Particles from Cosmic-ray Production*, *Phys. Rev. D* **102** (2020) 115032 [[2002.11732](#)].

[48] C.A. Argüelles Delgado, K.J. Kelly and V. Muñoz Albornoz, *Millicharged particles from the heavens: single- and multiple-scattering signatures*, *JHEP* **11** (2021) 099 [[2104.13924](#)].

[49] M. Kachelriess and J. Tjemsland, *Meson production in air showers and the search for light exotic particles*, *Astropart. Phys.* **132** (2021) 102622 [[2104.06811](#)].

[50] M. Du, R. Fang and Z. Liu, *Millicharged particles from proton bremsstrahlung in the atmosphere*, *JHEP* **08** (2024) 174 [[2211.11469](#)].

[51] H. Wu, E. Hardy and N. Song, *Searching for heavy millicharged particles from the atmosphere*, *Phys. Rev. D* **110** (2024) 115037 [[2406.01668](#)].

[52] S. Tulin, *New weakly-coupled forces hidden in low-energy QCD*, *Phys. Rev. D* **89** (2014) 114008 [[1404.4370](#)].

[53] B. Batell, P. deNiverville, D. McKeen, M. Pospelov and A. Ritz, *Leptophobic Dark Matter at Neutrino Factories*, *Phys. Rev. D* **90** (2014) 115014 [[1405.7049](#)].

[54] D.E. Soper, M. Spannowsky, C.J. Wallace and T.M.P. Tait, *Scattering of Dark Particles with Light Mediators*, *Phys. Rev. D* **90** (2014) 115005 [[1407.2623](#)].

[55] B.A. Dobrescu and C. Frugueule, *GeV-Scale Dark Matter: Production at the Main Injector*, *JHEP* **02** (2015) 019 [[1410.1566](#)].

[56] C. Kouvaris and J. Pradler, *Probing sub-GeV Dark Matter with conventional detectors*, *Phys. Rev. Lett.* **118** (2017) 031803 [[1607.01789](#)].

[57] L. Carloni and T. Sjostrand, *Visible Effects of Invisible Hidden Valley Radiation*, *JHEP* **09** (2010) 105 [[1006.2911](#)].

[58] L. Carloni, J. Rathsman and T. Sjostrand, *Discerning Secluded Sector gauge structures*, *JHEP* **04** (2011) 091 [[1102.3795](#)].

[59] Q.-B. Xie and X.-M. Liu, *Quark Production Rule in  $e^+e^- \rightarrow$  Two Jets*, *Phys. Rev. D* **38** (1988) 2169.

[60] Q. Wang, Z.-G. Si and Q.-B. Xie, *Simple understanding of the energy dependence of the B/M ratio and hadron multiplicities in  $e^+e^-$  annihilation*, *Int. J. Mod. Phys. A* **11** (1996) 5203.

[61] Z.-G. Si, Q.-B. Xie and Q. Wang, *Study of baryon anti-baryon rapidity correlation in  $e^+e^-$  annihilation by quark combination model*, in *7th International Workshop on Correlation and Fluctuations in Multiparticle Production*, pp. 203–211, 4, 1997, DOI [[hep-ph/9704271](#)].

[62] Z.-G. Si, Q. Wang and Q.-B. Xie, *Probability of color rearrangement at partonic level in hadronic  $W^+W^-$  decays*, *Phys. Lett. B* **401** (1997) 107 [[hep-ph/9704226](#)].

[63] Z.-G. Si, Q.-B. Xie and Q. Wang, *Study of baryon anti-baryon rapidity correlation in  $e^+e^-$  annihilation by quark combination model*, *Commun. Theor. Phys.* **28** (1997) 85.

[64] JUNO Collaboration, *Neutrino Physics with JUNO*, *J. Phys. G* **43** (2016) 030401 [[1507.05613](#)].

[65] JUNO Collaboration, *JUNO physics and detector*, *Prog. Part. Nucl. Phys.* **123** (2022) 103927 [[2104.02565](#)].

[66] JUNO Collaboration, *First measurement of reactor neutrino oscillations at JUNO*, [2511.14593](#).

[67] J. Berger, *A Module for Boosted Dark Matter Event Generation in GENIE*, [1812.05616](#).

[68] J. Berger and Z. Orr, *Resonant scattering of boosted Dark Matter*, *JHEP* **12** (2025) 031 [[2509.02678](#)].

[69] C. Andreopoulos et al., *The GENIE Neutrino Monte Carlo Generator*, *Nucl. Instrum. Meth. A* **614** (2010) 87 [[0905.2517](#)].

[70] C. Andreopoulos, C. Barry, S. Dytman, H. Gallagher, T. Golan, R. Hatcher et al., *The GENIE Neutrino Monte Carlo Generator: Physics and User Manual*, [1510.05494](#).

[71] T. Sjostrand, S. Mrenna and P. Skands, *PYTHIA 6.4 Physics and Manual*, *JHEP* **0605** (2006) 026 [[hep-ph/0603175](#)].

[72] K. Asai, A. Das, J. Li, T. Nomura and O. Seto, *Chiral Z' in FASER, FASER2, DUNE, and ILC beam dump experiments*, *Phys. Rev. D* **106** (2022) 095033 [[2206.12676](#)].

[73] PARTICLE DATA GROUP Collaboration, *Review of particle physics*, *Phys. Rev. D* **110** (2024) 030001.

[74] A. Fedynitch, R. Engel, T.K. Gaisser, F. Riehn and T. Stanev, *Calculation of conventional and prompt lepton fluxes at very high energy*, *EPJ Web Conf.* **99** (2015) 08001 [[1503.00544](#)].

[75] T.K. Gaisser, *Spectrum of cosmic-ray nucleons, kaon production, and the atmospheric muon charge ratio*, *Astropart. Phys.* **35** (2012) 801 [[1111.6675](#)].

[76] A. Fedynitch, F. Riehn, R. Engel, T.K. Gaisser and T. Stanev, *Hadronic interaction model sibyll 2.3c and inclusive lepton fluxes*, *Phys. Rev. D* **100** (2019) 103018 [[1806.04140](#)].

[77] J.M. Picone, A.E. Hedin, D.P. Drob and A.C. Aikin, *Nrlmsise-00 empirical model of the atmosphere: Statistical comparisons and scientific issues*, *Journal of Geophysical Research: Space Physics* **107** (2002) SIA 15 [<https://agupubs.onlinelibrary.wiley.com/doi/pdf/10.1029/2002JA009430>].

[78] J. Alwall, R. Frederix, S. Frixione, V. Hirschi, F. Maltoni, O. Mattelaer et al., *The automated computation of tree-level and next-to-leading order differential cross sections, and their matching to parton shower simulations*, *JHEP* **07** (2014) 079 [[1405.0301](#)].

[79] A. Alloul, N.D. Christensen, C. Degrande, C. Duhr and B. Fuks, *FeynRules 2.0 - A complete toolbox for tree-level phenomenology*, *Comput. Phys. Commun.* **185** (2014) 2250 [[1310.1921](#)].

[80] B. von Krosigk, L. Neumann, R. Nolte, S. Röttger and K. Zuber, *Measurement of the proton light response of various LAB based scintillators and its implication for supernova neutrino detection via neutrino-proton scattering*, *Eur. Phys. J. C* **73** (2013) 2390 [[1301.6403](#)].

[81] J.F. Acevedo, J. Berger and P.B. Denton, *Dark matter raining on DUNE and other large volume detectors*, *JHEP* **11** (2024) 011 [[2407.01670](#)].

[82] NA62 Collaboration, *Search for production of an invisible dark photon in  $\pi^0$  decays*, *JHEP* **05** (2019) 182 [[1903.08767](#)].

[83] NA62 Collaboration, *Searches for hidden sectors using  $K^+ \rightarrow \pi^+ X$  decays*, *JHEP* **11** (2025) 143 [[2507.17286](#)].

- [84] M. Honda, T. Kajita, K. Kasahara, S. Midorikawa and T. Sanuki, *Calculation of atmospheric neutrino flux using the interaction model calibrated with atmospheric muon data*, *Phys. Rev. D* **75** (2007) 043006 [[astro-ph/0611418](#)].
- [85] M. Honda, T. Kajita, K. Kasahara and S. Midorikawa, *Improvement of low energy atmospheric neutrino flux calculation using the JAM nuclear interaction model*, *Phys. Rev. D* **83** (2011) 123001 [[1102.2688](#)].
- [86] M. Honda, M. Sajjad Athar, T. Kajita, K. Kasahara and S. Midorikawa, *Atmospheric neutrino flux calculation using the NRLMSISE-00 atmospheric model*, *Phys. Rev. D* **92** (2015) 023004 [[1502.03916](#)].
- [87] R. Diurba and H. Kolešová, *Prospects of detecting cosmic ray up-scattered dark matter with DUNE*, *JHEP* **07** (2025) 202 [[2504.16996](#)].